J Solid State Electrochem (2007) 11:1385–1390
DOI 10.1007/s10008-007-0317-1

ORIGINAL PAPER

Co-synthesis of nano-sized LSM–YSZ composites with enhanced electrochemical property

Jung-Hyun Kim · Rak-Hyun Song · Jong-Hee Kim · Tak-Hyoung Lim · Yang-Kook Sun · Dong-Ryul Shin

Received: 29 December 2006 / Revised: 27 February 2007 / Accepted: 22 March 2007 / Published online: 14 April 2007

Abstract Nano-sized LSM–YSZ composite was co-synthesized by a glycine–nitrate process (GNP). Transmission electron microscopy revealed that the as-prepared LSM–YSZ particles consist of nano-sized powders with a dominant YSZ phase. Backscatter electron image shows that LSM and YSZ phases were regularly dispersed within the composite. Alternating current impedance measurement revealed that the co-synthesized LSM–YSZ electrode shows lower polarization resistance and activation energy than the physically mixed LSM–YSZ electrode. This electrochemical improvement would be attributed to the increase in three-phase boundary and good dispersion of LSM and YSZ phases within the composite.

Keywords LSM–YSZ composite · Cathode · Glycine–nitrate process · Solid oxide fuel cell (SOFC)

Introduction

Perovskite $La_{1-x}Sr_xMnO_{3-\delta}$ is one of the most promising candidate as a cathode material for solid oxide fuel cell (SOFC) because of its high stability, good electrocatalytic activity for oxygen reduction, and thermal expansion compatibility with YSZ [1–8]. When the operating temperature is reduced, unfortunately, dramatic increase in interfacial polarization resistances between LSM and YSZ becomes a critical problem. In recent studies, mixture of LSM and YSZ was employed as a functionally graded cathode that lay between LSM cathode and YSZ electrolyte and showed superior electrochemical performance to the single LSM. Such an improvement resulted from the increase in triple-phase boundary (TPB) length that consists of electrode/electrolyte/gas interface [8–12]. Therefore, there have been intensive researches on the increase in TPB length. This can be achieved by optimizing the LSM/YSZ ratio (according to the percolation theory) or by employing small particles of the LSM and YSZ.

Conventional solid-state reaction method, however, is not suitable for obtaining small particles of LSM or YSZ because it requires high calcination temperature, which significantly reduces the effective TPB length. Accordingly, various synthetic methods were introduced to obtain nano-sized LSM or YSZ, for example, sol–gel method [13–16], combustion method [17, 18], hydrothermal method [19], and spray-pyrolysis method [20]. Among them, glycine–nitrate process (GNP) is an attractive combustion method by which fine and well-crystallized powders could be obtained. In the GNP method, auto-ignition reaction between metal nitrates (oxidizers) and a glycine (fuel) provides heat for the synthesis of desired product.

Recently, there have been new trials to synthesize LSM–YSZ composite together by Pechini and spray-pyrolysis methods [21, 22]. Nano-sized LSM–YSZ composite powders were successfully obtained by those methods, although secondary phase such as $LaYO_3$ was often induced depending on synthetic conditions. In this work, we

This paper is dedicated to Professor Su-Il Pyun on the occasion of his 65th birthday.

J.-H. Kim · R.-H. Song (✉) · J.-H. Kim · T.-H. Lim · D.-R. Shin
New Energy Research Department,
Korea Institute of Energy Research,
71-2 Jang-dong, Yuseong-gu,
Daejeon 305-600, Republic of Korea
e-mail: rhsong@kier.re.kr

J.-H. Kim · Y.-K. Sun
Department of Chemical Engineering,
Hanyang University,
Seungdong-gu,
Seoul 133-791, Republic of Korea

synthesized LSM–YSZ composite powder by GNP method for the first time in our knowledge. Co-synthesis of LSM–YSZ composite by GNP has several advantages as follows; as the LSM–YSZ composite phase was formed from their mixed solution, it is highly probable that each phase was well dispersed with inter-atomic scale. This would be beneficial in increasing TPB length in the composite. In addition, gas product of the GNP synthesis results in large porosity within the LSM–YSZ composite. Finally, we could obtain nano-sized LSM–YSZ product in a large quantity by a very simple way at relatively low temperature. We also compared the electrochemical properties of the co-synthesized LSM–YSZ with a physically mixed LSM–YSZ.

Experimental

LSM–YSZ composite powder was co-synthesized by GNP method. The chemical formula of LSM and YSZ are $(La_{0.85}Sr_{0.15})_{0.9}MnO_3$ and $Y_{0.15}Zr_{0.85}O_{1.92}$, respectively, and the weight ratio of LSM and YSZ was 6:4 in the composite. Stoichiometric amount of $La(NO_3)_3{\cdot}6H_2O$, $Sr(NO_3)_2$, $Mn(NO_3)_2{\cdot}4H_2O$, $Y(NO_3)_3{\cdot}6H_2O$, and $Zr(NO_3)_2{\cdot}6H_2O$ were dissolved together in distilled water. Proper amount of glycine (NH_2CH_2COOH) was added to the solution and then heated. As the water was evaporated, transparent viscous gel was formed, followed by its abrupt auto-ignition. The vigorous exothermic reaction ended within a few seconds, and voluminous powders were obtained. The powders were calcined at various temperatures. For comparison, $(La_{0.85}Sr_{0.15})_{0.9}MnO_3$ and $Y_{0.15}Zr_{0.85}O_{1.92}$ were individually synthesized by GNP method.

Powder X-ray diffraction (XRD, Rint-2000, Rigaku, Japan) measurement using Cu Kα radiation was employed to identify the crystalline phase of the synthesized materials. XRD data were obtained at 2θ=20 to 80°, with a step size of 0.03°. From the XRD data, lattice parameters were calculated by a least squares method. The morphology and backscatter electron images of powders were observed using a scanning electron microscope with energy dispersive spectroscope (SEM, JSM 6400, JEOL, Japan). For a clear backscatter electron image, LSM–YSZ composite powders were pressed into pellet and calcined at 1,400 °C for 5 h, followed by polishing and thermal etching at 1,200 °C.

For electrochemical test, a working electrode was prepared by screen printing LSM–YSZ slurry on the one side of commercial YSZ plate (0.2 mm thick, Tosoh, Japan). The electrodes were dried at 100 °C, and another thin layer of LSM was screen printed above the LSM–YSZ layer, followed by sintering at 1,150 °C for 2 h. Each layer was 5 μm thick. Pt mesh was attached with Pt paste on the opposite side of YSZ plate as a counter electrode. Pt reference was placed at interval of 4 mm from the working electrode.

Alternating current (AC) impedance was measured by a Solartron 1260 frequency response analyzer coupled with a Solartron 1287 electrochemical interface in the frequency range from 5×10^5 to 10^{-2} Hz using an amplitude of 70 mV. The measured data were fitted with a ZVIEW software.

Results and discussion

On the synthesis of LSM–YSZ composite material using a GNP method, glycine acts as a fuel of which violent exothermic reaction provides heat for the phase formation. In GNP method, an amount of the glycine is an important factor to obtain a desired product. Therefore, we synthesized LSM and YSZ individually by the GNP method using appropriate amounts of glycine. To obtain pure LSM and/or YSZ phases by GNP method, minimum glycine amount was calculated by the following chemical equations where oxygen in air does not participate in the reactions:

$$\begin{aligned} &0.765\ La(NO_3)_3\cdot 6H_2O + 0.135\ Sr(NO_3)_2 \\ &+ 1\ Mn(NO_3)_2\cdot 4H_2O + 2.3767\ C_2H_5NO_2 \\ &\rightarrow (La_{0.85}Sr_{0.15})_{0.9}MnO_3 + 4.753\ CO_2 \\ &+ 14.532\ H_2O + 3.471\ N_2 \end{aligned} \quad (1)$$

$$\begin{aligned} &0.92\ ZrO(NO_3)_3\cdot 6H_2O + 0.16\ Y(NO_3)_3\cdot 6H_2O \\ &+ 0.089\ C_2H_5NO_2 \\ &\rightarrow (ZrO_2)_{0.92}(Y_2O_3)_{0.08} + 0.178\ CO_2 \\ &+ 6.702\ H_2O + 1.204\ N_2 \end{aligned} \quad (2)$$

When extra amount of glycine was used, oxygen in air participated in the reaction that led to more vigorous auto-ignition of gels [23, 24]. Large amount of glycine, however, often hinders formation of the desired phase due to residual carbon. Therefore, we varied the glycine amount and could obtain pure LSM and YSZ phases using 2.3767 and 1 mol of glycine, respectively, per 1 mol of each final product. From this value, we decided to use 3.3767 mol of glycine to obtain 1 mol of LSM–YSZ composite material.

On the synthesis of LSM–YSZ composite, extremely light and voluminous powders were obtained after the violent combustion reaction of glycine. Figure 1 shows a SEM image of the resulting powders. LSM–YSZ composite powders consist of macro-sized particles with large pores due to a sudden evaporation of gas products such as CO_2, H_2O, and N_2 during exothermic reaction. In fact, the macro-sized secondary particles were agglomerates of fine primary

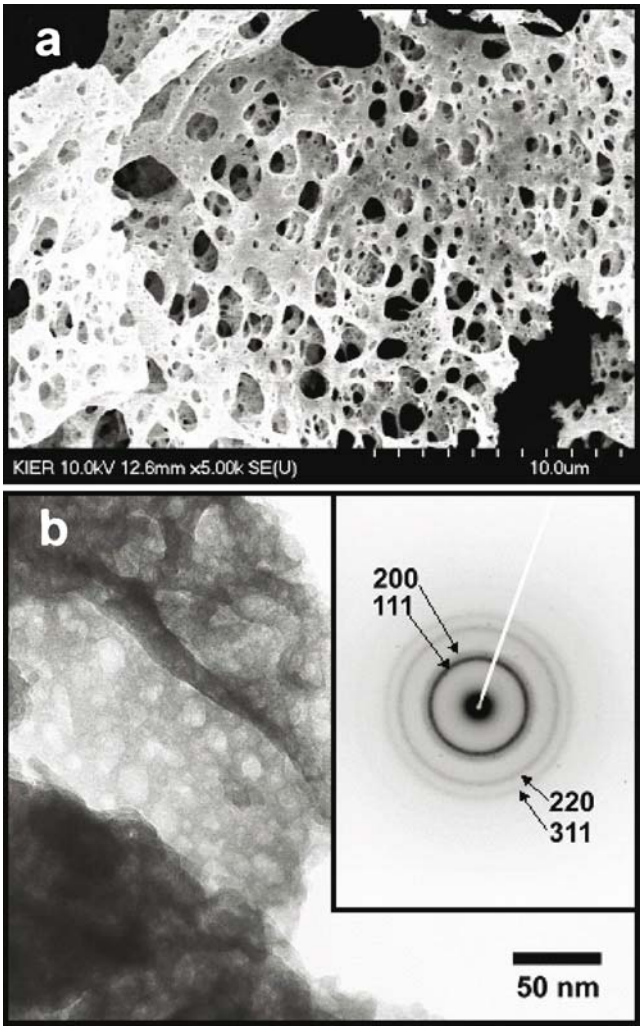

Fig. 1 **a** SEM image and **b** bright field image of the as-prepared LSM–YSZ composite

particles, which could not be clearly observed even at a high magnification of 10^5. Therefore, to further ascertain the prepared powder, transmission electron microscopy (TEM) analysis was carried out. Figure 1b shows the bright field image of the prepared LSM–YSZ powders. The primary particle size was less than 20 nm, and the individual particles were severely agglomerated. Electron diffraction pattern obtained from individual particles is also shown in the inset figure. Ring-shaped diffractions indicated that the as-prepared powders have nano-sized polycrystalline structure and could be indexed by face-centered cubic structure. This result agreed well with the XRD pattern of the as-prepared powders in Fig. 2(a). The as-prepared LSM–YSZ composite powders showed broad XRD peaks that roughly correspond to a fluorite YSZ phase as shown in the TEM analysis. However, perovskite LSM phase was not observed in the as-prepared LSM–YSZ composite by the GNP method. When LSM or YSZ was individually synthesized by the GNP method, we could obtain clear perovskite or fluorite phase (not shown here). Here, we noted that the degree of auto-ignition of metal nitrates and glycine during LSM and YSZ formation was quite different. The metal nitrates in the LSM reaction showed a sudden violent explosion of powders during combustion reaction that finished within a few seconds, whereas auto-ignition of the metal nitrates in the YSZ formation was very gentle, having tiny glowing flints propagating within the mixture until the reaction completes. When we co-synthesized LSM–YSZ composite, auto-ignition was very gentle like that of YSZ. Therefore, we infer that phase formation of LSM was hindered by the slow combustion rate of YSZ, which resulted in the dominant YSZ phases in Figs. 1b and 2(a).

The as-prepared LSM–YSZ composite powders were calcinated at various temperatures ranging from 800 to 1,200 °C, and their XRD patterns are shown in Fig. 2(b–f). The LSM perovskite phase was observed at 800 °C from its XRD pattern in Fig. 2(b). At low calcination temperatures of 800–900 °C, XRD peaks of perovskite phase showed narrow full width at half maximum (FWHM), while those of fluorite phase were relatively broad in Fig. 2(b and c). This result indicates that LSM particles grow better than YSZ at low temperature. At a temperature higher than 1,000 °C, however, YSZ also showed narrow FWHM. In this temperature range, we could not find secondary phases such as $La_2Zr_2O_7$ or $Sr_2Zr_2O_7$ that easily formed between LSM and YSZ interface [25, 26].

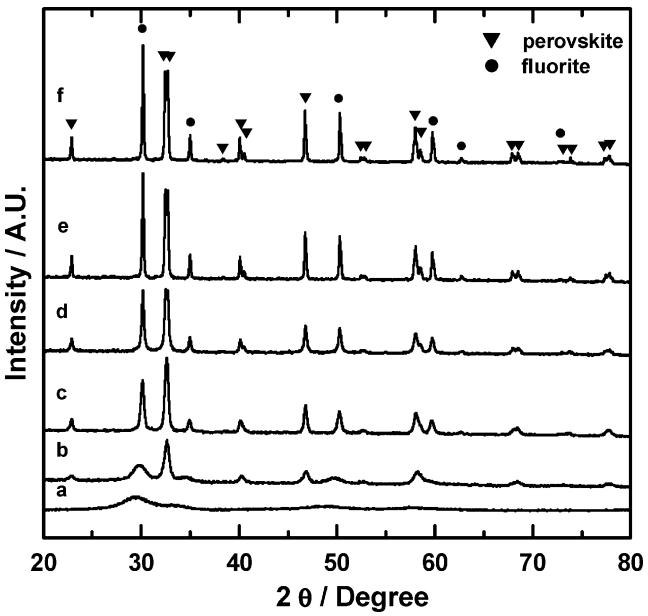

Fig. 2 XRD profiles of the co-synthesized LSM–YSZ composite powders calcinated at various temperatures; (*a*) as-prepared, (*b*) 800 °C, (*c*) 900 °C, (*d*) 1,000 °C, (*e*) 1,100 °C, and (*f*) 1,200 °C

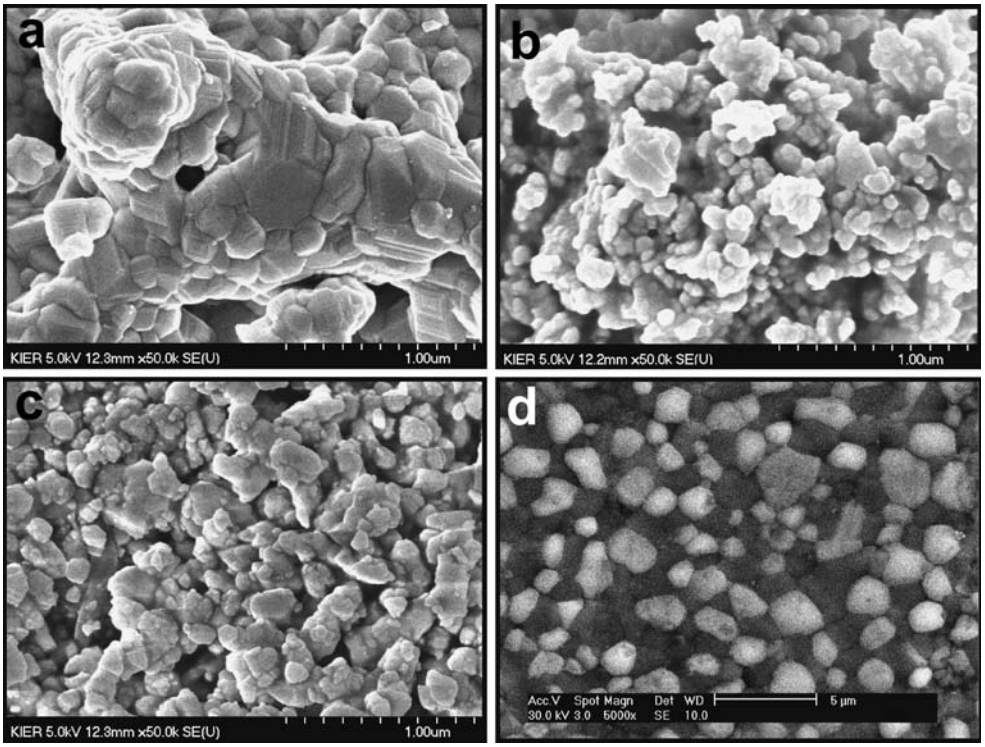

Fig. 3 SEM images of **a** single LSM, **b** single YSZ, and **c** co-synthesized LSM–YSZ composite calcinated at 1,000 °C for 5 h. And, **d** backscatter electron image of the co-synthesized LSM–YSZ composite sintered at 1,400 °C for 5 h

Morphology and particle size of the LSM, YSZ, and LSM–YSZ composite powders were compared. Fig. 3a–c shows SEM images of LSM, YSZ, and LSM–YSZ composite powders, respectively, calcinated at 1,000 °C for 5 h. The pure LSM powders were approximately 200–300 nm, while the pure YSZ powders were less than 100 nm in diameter. This result shows that LSM particles grow much faster than YSZ and agrees well with our XRD

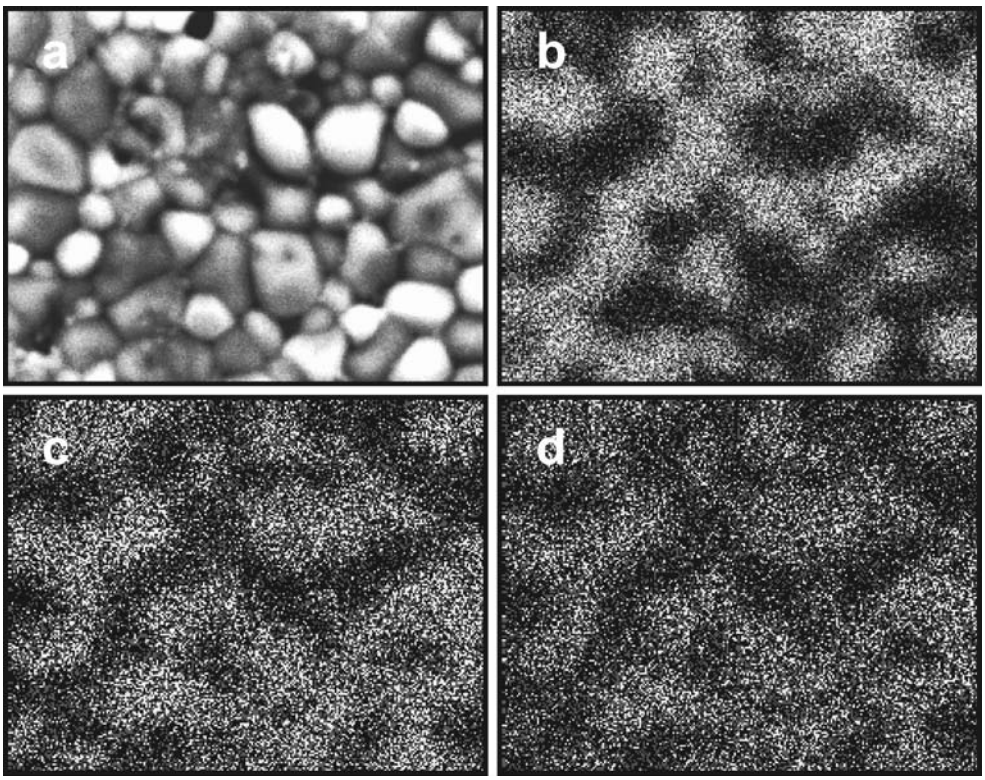

Fig. 4 SEM image of **a** the surface of LSM–YSZ composite sintered at 1,400 °C for 5 h and its EDS spots of **b** Zr–Lα, **c** La–Lα, and **d** Mn–Kα, respectively

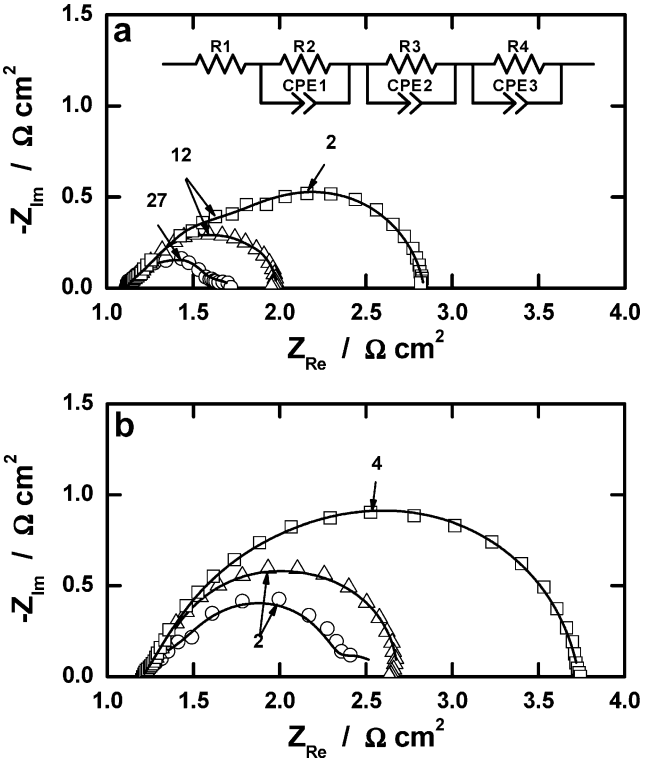

Fig. 5 Nyquist plot of LSM/LSM–YSZ/YSZ electrodes under various oxygen partial pressures at 750 °C; **a** co-synthesized LSM–YSZ composite and **b** physically mixed LSM–YSZ composite. *Open symbols* represent measurement point, and *solid line* indicates fitting result (*circle* 1 bar, *triangle* 0.2 bar, *square* 0.01 bar)

results in Fig. 2. In case of the LSM–YSZ composite powders, particles were 100–200 nm in diameter. Although we could not distinguish each particle in the LSM–YSZ composites calcined below 1,200 °C, it is evident that LSM particles in LSM–YSZ composite were much smaller than single LSM. As the LSM–YSZ composite phase was formed from their mixed solution, each phase may effectively suppress the growth of the other phase.

To observe the distribution of LSM and YSZ phases in the composite material, backscatter electron image was measured in Fig. 3d. For clear image, composite powders were pressed into pellet followed by sintering at 1,400 °C for 5 h. LSM (bright part) and YSZ (dark part) were clearly distinguished and regularly dispersed in the composite without severe agglomeration of each phase. We also observed the distribution of each element in the composite by energy dispersive X-ray spectroscopy (EDS) mapping. For a specific region in Fig. 4a, Zr–Lα, La–Lα, and Mn–Kα were spotted in Fig. 4b–d. Although LSM and YSZ phases coexisted in the vertical direction, each phase was clearly distinguished into separated domains. In the literature, Mn ions could be incorporated into YSZ to form a solid solution [27–30]. The maximum solubility of Mn in 8YSZ was about 10 mol% at 1,500 °C. However, our EDS result clearly shows that Mn–Kα spots have the same domains as that of La–Lα. And this domain was contrary to that of Zr–Lα. Therefore, it is reasonable that the possible Mn dissolution into YSZ phase was negligible in our LSM–YSZ composite material.

We studied the electrochemical performance of nano-sized LSM–YSZ composite by AC impedance spectroscopy. For comparison, physical mixture of LSM and YSZ (6:4 in weight ratio) was prepared by ball milling. AC impedance was measured between 700 and 850 °C by varying oxygen partial pressure from 1 to 0.01 bar. The spectra of LSM–YSZ electrodes consist of three suppressed semicircles as illustrated in Fig. 5. Inset in Fig. 5a shows the corresponding model circuit for the LSM–YSZ composite. R1 represents a resistance between reference electrode (RE) and working electrode (WE). The R1 includes the contact resistance between Pt and WE, resistance of WE, and the resistance of Pt wire. R2 and R3 have been interpreted as inter-grain resistance and grain boundary resistance or Pt/LSM and LSM/LSM–YSZ interface resistance [31]. The low-frequency semicircle, R4, showed a strong dependence on oxygen partial pressure and is assigned to the charge transfer resistance [31–33]. This resistance was independent of the gas flow rate. All impedance plots were fitted properly by this model circuit, and the fitting results were illustrated as a solid line in Fig. 5, showing a good agreement with the measurement. Both the co-synthesized and ball-milled LSM–YSZ showed strong dependence of R4 on the oxygen partial pressure. Although the physical mixture of LSM–YSZ did not show the clear separation of each semicircle in Fig. 5b, our fitting results showed that low frequency arc was larger than high-frequency arc at low temperature and low oxygen partial

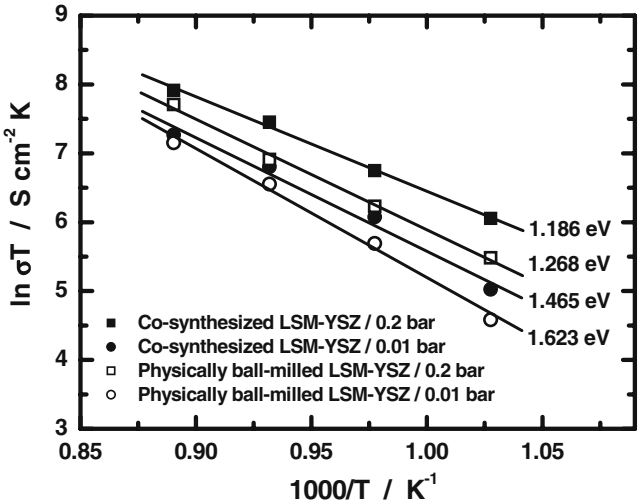

Fig. 6 Arrhenius plot of the electric conductivity for co-synthesized and physically mixed LSM–YSZ electrodes under oxygen partial pressures of 0.2 and 0.01 bar

pressure. This result indicates that charge transfer process limits the LSM–YSZ electrode reaction. It is notable that the co-synthesized LSM–YSZ composite shows lower polarization resistance (R_p) value than ball-milled LSM–YSZ in Fig. 5. As confirmed by SEM, co-synthesis of the LSM–YSZ composite effectively suppressed the particle growth of LSM in Fig. 3. In addition, LSM and YSZ phases would be dispersed better in the chemically mixed state (co-synthesis) than the physically mixed one (ball milling). The small particle size of LSM and good dispersion of each particle in the co-synthesized LSM–YSZ would lead to the extended TPB length than the ball-milled one. This extended TPB length is advantageous to the charge transfer reaction resulting in low R_p values.

From the R_p value, we calculated the interface conductivity, σ, that correlated with the oxygen reduction rates at the interface of LSM/YSZ. Figure 6 shows the temperature dependence of conductivity. Each set of data was fitted with least squares method and illustrated as solid lines. The corresponding activation energy (E_a) was also indicated in Fig. 6. The co-synthesized LSM–YSZ composite showed a lower E_a value (1.186 eV) than the ball-milled one (1.268 eV) in air. These E_a values are in good agreement with the reported one [34, 35]. Even at low oxygen partial pressure of 0.01 bar, the co-synthesized LSM–YSZ showed lower E_a values than the ball-milled LSM–YSZ. The low polarization resistance and activation energy of the co-synthesized LSM–YSZ composite would be attributed to the well-dispersed LSM and YSZ nanoparticles that effectively extended the TPB length.

Conclusion

We synthesized LSM, YSZ, and their composite by GNP method. At first, we searched for the proper amount of glycine to obtain pure LSM and YSZ phases. Then, LSM–YSZ composite material was co-synthesized in a batch. The co-synthesized LSM–YSZ composite consists of smaller particles than single LSM, and each particle was regularly dispersed in the composite. The electrochemical property of the co-synthesized LSM–YSZ composite was compared with the physically mixed one. AC impedance measurement revealed that the co-synthesized LSM–YSZ electrode had smaller polarization resistance and lower activation energy (E_a) than the ball-milled LSM–YSZ electrode. This electrochemical improvement would be attributed to the increase in TPB where the charge transfer reaction can occur.

References

1. Singhal SC (2000) Solid State Ionics 135:305
2. Minh NQ (1993) J Am Ceram Soc 76:563
3. Horita T, Yamaji K, Ishikawa M, Sakai N, Yokokawa H, Kawada T, Kato T (1998) J Electrochem Soc 145:3196
4. Mizusaki J, Yonemura Y, Kamata H, Ohyama K, Mori N, Takai H, Tagawa H, Dokiya M, Naraya K, Sasamoto T, Inaba H, Hashimoto T (2000) Solid State Ion 132:167
5. Van Heuveln FH, Bouwmeester HJM, Van Berkel FPF (1997) J Electrochem Soc 144:126
6. Van Heuveln FH, Bouwmeester HJM (1997) J Electrochem Soc 144:134
7. Zheng F, Pederson LR (1999) J Electrochem Soc 146:2810
8. Murray EP, Tsai T, Barnett SA (1998) Solid State Ion 110:235
9. Tsai T, Barnett SA (1997) Solid State Ion 93:207
10. Jorgensen MJ, Primdahl S, Mogensen M (1999) Electrochim Acta 44:4195
11. Ostergard MJL, Clausen C, Bagger C, Mogensen M (1995) Electrochim Acta 40:1971
12. Juhl M, Primdahl S, Manon C, Mogensen M (1996) J Power Sources 61:173
13. Licci F, Turilli G, Ferro P, Ciccarone A (2003) J Am Ceram Soc 86:413
14. Egger P, Sorarù GD, Dirè S (2004) J Eur Ceram Soc 24:1371
15. Robert CL, Ansart F, Deloget C, Gaudon M, Rousset A (2001) Mater Res Bull 36:2083
16. Okubo T, Nagamoto H (1995) J Mater Sci 30:749
17. Taguchi H, Mastuda D, Nagao M, Tanihata K, Miyamoto Y (1992) J Am Ceram Soc 75:201
18. Taguchi H, Sugita A, Nagao M (1996) J Solid State Chem 121:495
19. Barnabé A, Gaudon M, Bernard C, Laberty C, Durand B (2004) Mater Res Bull 39:725
20. Matsizaki Y, Hishinuma M, Yasuda I (1999) Thin Solid Films 340:72
21. Gaudon M, Laberty-Robert C, Ansart F, Stevens P, Rousset A (2003) Solid State Sci 5:1377
22. Marinković ZV, Manćić L, Cribier JF, Ohara S, Fukui T, Milošević O (2004) Mater Sci Eng A 375:615
23. Deshpande K, Mukasyan A, Varma A (2004) Chem Mater 16:4896
24. Toniolo JC, Lima MD, Takimi AS, Bergmann CP (2005) Mater Res Bull 40:561
25. Lee HY, Oh SM (1996) Solid State Ion 90:133
26. Kindermann L, Das D, Bahadur D, Weib R, Nickel H, Hipert K (1997) J Am Ceram Soc 80:909
27. Mori M, Abe T, Itoh H, Yamamoto O, Shen GQ, Takeda Y, Imanishi N (1999) Solid State Ion 123:113
28. Appel CC (1995) Ionics 1:406
29. Kim JH, Choi GM (2000) Solid State Ion 130:157
30. Matraszek A, Miller M, Singheiser L, Hilpert K (2004) J Eur Ceram Soc 24:2649
31. Co AC, Xia SJ, Birss VI (2005) J Electrochem Soc 152:A570
32. Wang S, Jiang Y, Zhang Y, Yan J, Li W (1998) Solid State Ion 113:291
33. Kamata H, Hosaka A, Mizusaki J, Tagawa H (1998) Solid State Ion 106:237
34. Zhao H, Huo L, Gao S (2004) J Power Sources 125:149
35. Hart NT, Brandon NP, Day MJ, Lapena-Rey N (2002) J Power Sources 106:42